Polymer 51 (2010) 5799–5806

Contents lists available at ScienceDirect

Polymer

journal homepage: www.elsevier.com/locate/polymer

Composition-dependent phase segregation and cocrystallization behaviors of blends of metallocene-catalyzed octene-LLDPE(D) and LDPE(H)

Tae Joo Shin [a,1], Byeongdu Lee [b,1], Baik Shuk Seong [c], Young Soo Han [c], Chang-Hee Lee [c], Hyun Hoon Song [d], Richard S. Stein [e], Moonhor Ree [a,*]

[a] Pohang Accelerator Laboratory, Department of Chemistry, Center for Electro-Photo Behaviors in Advanced Molecular Systems, Polymer Research Institute, and BK School of Molecular Science, Pohang University of Science & Technology, Pohang 790-784, Republic of Korea
[b] Advanced Photon Source, Argonne National Laboratory, Argonne, IL 60439, USA
[c] Korea Atomic Energy Research Institute, HANARO Center, Daejeon 305-600, Republic of Korea
[d] Department of Advanced Materials, Hannam University, Jeonmin-dong, Yuseong-gu, Daejeon 305-811, Republic of Korea
[e] Polymer Research Institute and Department of Polymer Science and Engineering, University of Massachusetts, Amherst, MA 01003, USA

ARTICLE INFO

Article history:
Received 20 July 2010
Received in revised form
29 September 2010
Accepted 30 September 2010
Available online 8 October 2010

Keywords:
Small angle neutron scattering (SANS)
Small angle X-ray scattering (SAXS)
O-*m*LLDPE/LDPE blend

ABSTRACT

The morphological structures of slowly cooled blends of deuterated metallocene-catalyzed octene linear low-density polyethylene (O-*m*LLDPE(D)), and hydrogenous low-density polyethylene (LDPE(H)) were studied by using small angle neutron scattering in combination with complementary small angle X-ray scattering and differential scanning calorimetry. The phase segregation, which is more nanoscale than macroscale, and cocrystallization behaviors were found to vary with the blend composition. Phase-segregated O-*m*LLDPE(D) lamellae are predominantly formed in LDPE(H)-rich compositions. In contrast, few segregated O-*m*LLDPE(D) lamellae form in O-*m*LLDPE(D)-rich compositions, and instead O-*m*LLDPE(D) lamellar stacks are extensively cocrystallized with LDPE(H) mostly in the interlamellar amorphous region.

1. Introduction

Linear low-density polyethylene (LLDPE) is a linear polyethylene (PE) containing alkyl short-chain branches (SCBs) [1,2] that are introduced through the insertion of α-olefins (1-butene, 1-hexene, 1-octene, etc.) during the polymerization of ethylene. In general, LLDPEs are synthesized by using Ziegler–Natta catalysts or homogeneous metallocene catalysts. Ziegler–Natta catalyzed LLDPEs (ZN-LLDPEs) are known to exhibit liquid–liquid phase separation even in the case of 'pure' LLDPE [3–7] because of their intrinsic wide molecular weight distribution and wide branch content distribution [8]. As a result, ZN-LLDPE products often exhibit melt fracture, surface distortion, and significant deterioration in their mechanical and optical performances. In comparison, homogeneous metallocene-catalyzed LLDPEs (*m*LLDPEs) have very narrow molecular weight distributions and sparse long-chain branches (LCBs), so their physical and mechanical properties are superior to those of ZN-LLDPEs. However, they often have poor processibilities due to their high viscosities, which mean that high melt pressures and high motor loads are required during extrusion processing [9]. Therefore, further processing steps such as blending with other polymers are necessary for *m*LLDPEs to meet the requirements for industrial applications. Blending *m*LLDPEs with low-density polyethylene (LDPE) is one promising method for improving their poor processibility because LDPE contains a significant amount of LCBs [10–12]. In this regard, detailed studies of the miscibility and crystallization behavior of *m*LLDPE/LDPE blends are required to characterize and improve polymer processing and blend properties.

The strong influences on miscibility and crystallization of molecular weight, molecular weight distribution, composition distribution, branch type, branch content, and branch content distribution along the backbone have been widely studied [9,13–16]. In particular, a series of studies of cocrystallization and phase segregation in blends of deuterated (D) HDPEs and hydrogenous (H) LLDPEs have been reported [17]. In these studies, it was concluded that H and D species cocrystallize into the same crystalline lattices in a statistically random arrangement and that the crystallization behavior is strongly influenced by the degree of branching of the hydrogenous LLDPEs, the composition (blend content), and the crystallization rate of the two components, as well as by the balance between the thermodynamic and kinetic factors of the two components. Recently, we reported that

* Corresponding author. Tel.: +82 54 279 2120; fax: +82 54 279 3399.
E-mail address: ree@postech.edu (M. Ree).
[1] TJS and BL contributed equally to this work.

0032-3861/$ – see front matter © 2010 Elsevier Ltd. All rights reserved.
doi:10.1016/j.polymer.2010.09.075

octene-*m*LLDPE and LDPE are miscible in both the melt state and the quenched solid state [18], which suggests that such blends are thermodynamically miscible. Moreover, we suggested that the two polymer components cocrystallize via fast crystallization from the melt state to the solid state because the radii of gyration of deuterated octene-*m*LLDPE (O-*m*LLDPE(D)) and hydrogenous LDPE (LDPE(H)) remain unchanged in the quenched solid state with respect to those of the melt state.

One of the most significant obstacles to the industrial use of PE blends is the phenomenon of phase segregation of the components of the blends, so research into the kinetic factors in their crystallization and phase behavior, and in particular during slow cooling, is of great importance. In the present study, the crystallization and phase behaviors of O-*m*LLDPE(D) and LDPE(H) blends under slow cooling conditions were studied by using small angle neutron and X-ray scattering (SANS and SAXS), as well as differential scanning calorimetry (DSC). The complex morphological structures of the blends at various compositions were investigated in detail.

2. Experimental section

2.1. Sample preparation

O-*m*LLDPE(D) and LDPE(H) samples were purchased from Exxon Chemical Company. The characteristics of the polyethylene samples and details can be found at Table 1. O-*m*LLDPE and LDPE (the total amount of the polymers was 0.3–1.0 g) were blended in 350 mL 1,2,4-trichlorobenzene containing about 0.1 g of 2,6-di-tert-butyl-4-methyl phenol (an antioxidant) at 180 °C under nitrogen and stirred for 2 h. Then, the solution was quickly coprecipitated in excess methanol at ice-water temperature, filtered on a fine glass filter, and washed with acetone. The washed sample was again immersed in several ml acetone containing 0.05 wt-% (corresponding to the total amount of the polymer mixture) of the antioxidant for a day, and then pre-dried under low vacuum (about 50 mmHg) at room temperature. The pre-dried sample was finally dried under high vacuum (less than 0.01 mmHg) at about 60 °C for a week. Then the blend samples were melt again on a Carver Press at 155 °C for 10–15 min and pressed to produce flat pellet-type specimens, which were then quenched into ice-water. During the specimen molding process, the cycle of pressurising the sample for a short time (for example, a half to 1 min) and subsequent releasing the pressure was conducted several times to remove any air-bubbles possibly trapped in the specimen. The obtained specimens were checked to have no air-bubbles by SAXS analysis before use in this study. The thickness of the blend specimens was controlled at 1.5 ± 0.01 mm. Slowly cooled polyethylene blends samples were prepared with 0.5 °C/min cooling rate from the melt state.

2.2. SANS and SAXS measurements

SANS data were collected at the HANARO SANS facility at the Korea Atomic Energy Research Institute by using an area detector with 64 × 64 cm^2 of active area, in which an element size is 25 mm^2. The wavelength, λ, of the neutron source was 8.29 Å and the sample-to-detector distance was about 4 m, resulting in a scattering vector range of 0.005 $Å^{-1} < q < 0.3$ $Å^{-1}$, where q is scattering vector defined as $q = 4\pi\cdot\sin\theta/\lambda$. Corrections for the instrumental background and detector efficiency were carried out prior to the radial averaging of the scattering profiles. The net intensity was converted to an absolute differential cross section per unit volume, $d\Sigma/d\Omega(q)$, by using pre-calibrated secondary silica standards. The cross sections of O-*m*LLDPE(H)/LDPE(H) blend samples were also measured in order to subtract the coherent and incoherent backgrounds. The coherent background arises mainly from void scattering and is negligible when $q > 0.012$ $Å^{-1}$. The incoherent background is a flat background [19] due to the incoherent cross section of ^1H, which can be subtracted with empirical methods [20]. As shown in eq (1), the scattering intensity of each sample (I_{sample}) was acquired by subtracting the transmission corrected ($\%T_{sample}/\%T_{cell}$) empty cell scattering (I_{cell}) from the observed scattering (I_{obs}). The sample transmittance ($\%T_{sample}$) is the ratio of the direct beam intensities measured with and without a sample, and was measured with the area detector for SANS with a beam-stop out of the beam direction.

$$I_{sample} = I_{obs} - \frac{\%T_{sample}}{\%T_{cell}} I_{cell} \tag{1}$$

The absolute scattering cross section, $(d\Sigma/d\Omega)_{total}$, was calculated with using the silica standard as a reference:

$$\left(\frac{d\sum}{d\Omega}\right)_{total} = \left(\frac{d\sum}{d\Omega}\right)_{silica} \frac{I_{sample}}{I_{silica}} \frac{\%T_{silica}}{\%T_{sample}} \frac{t_{silica}}{t_{sample}} \tag{2}$$

where $(d\Sigma/d\Omega)_{silica}$ is the absolute scattering cross section of silica, and I_i, $\%T_i$, and t_i represent the scattering intensity, transmission, and the thickness of i-component, respectively.

SAXS experiments were conducted at the SAXS Beamlines (4C1 and 4C2) [21,22] of Pohang Accelerator Laboratory [23] in Korea. A two-dimensional (2D) charge-coupled device (CCD) detector (Princeton Instruments, Inc., USA) consisting of 1152 × 1242 pixels was used for SAXS measurements. A sample-to-detector distance was set to about 1.4 m. The scattering angle and the absolute scattering intensity were respectively calibrated using lead stearate (d-spacing = 5.10 nm) and Lupolen standards as references. Each measured SAXS profile was circularly averaged.

The thermal behavior was studied via DSC using a Seiko DSC-220CU that was calibrated for temperature and melting enthalpy using indium and tin as standards. 10 °C/min of heating rate was applied to exclude any other crystallization during the heating scan. Degrees of crystallinity were calculated by comparison with the heat of fusion of a perfectly crystalline polyethylene, i.e., 289 J/g [24].

2.3. SANS data analysis

The coherent cross section, $(d\Sigma/d\Omega)_{coh}$, of a homogeneous polymer blend composed of hydrogenous (H) and deuterated (D) components is given by the following equation [19,20,25–27]:

$$\left(\frac{d\sum}{d\Omega}\right)_{coh} = \left(\frac{b_H}{v_H} - \frac{b_D}{v_D}\right)^2 S(q) \tag{3}$$

where b_H and b_D are the unit scattering length of hydrogenous and deuterated species, having -0.166×10^{-12} and 3.998×10^{-12} cm, respectively. v_H and v_D, representing the segment volume of each component, are 32.90 and 32.92 cm^3/mol at 145 °C, respectively. And $S(q)$ represents structure factor. The thermal expansion coefficient, 7.5×10^{-4}/°C, is assumed to be the same for both PE(H) and

Table 1
Molecular weight and density of polyethylene samples used in this study.

Sample	$\overline{M}_w$	$\overline{M}_n$	$\overline{M}_w/\overline{M}_n$	Density[a] (g/cm^3)
O-*m*LLDPE(D)[b]	94,800	52,700	1.8	1.1160
O-*m*LLDPE(H)[c]	96,000	56,500	1.7	0.9141
LDPE(H)[d]	286,000	17,900	16	0.9128

[a] Measured for quenched samples.
[b] Deuteration level was 94–95%. 3 mol% hexyl branched copolymer.
[c] 3 mol% hexyl branched copolymer.
[d] Contained 26 short branches/1000 carbon and 34 long branches/$\overline{M}_w$ (2.4 long branches/1000 carbon). Short and long branches mean branches containing >8 and ≤8 carbon atoms, respectively.

PE(D) above melting temperature [28]. According to the random phase approximation (RPA), the structure factor of a mixture of two components (H and D) in a single-phase state, or homogeneous mixture, is given by the following equation [19,20,25–27]:

$$\frac{1}{S(q)} = \frac{1}{\nu_D\phi_D N_D P_D(u)} + \frac{1}{\nu_H\phi_H N_H P_H(u)} - \frac{2\chi}{\nu} \tag{4}$$

where φ_i and N_i are the volume fraction and the degree of polymerization of ith component, respectively. χ is the Flory–Huggins interaction parameter, and ν is defined as $\nu=(\nu_H\nu_D)^{1/2}$. $P_i(u)$ is the normalized form factor of ith component, and it can be represented by the Debye function of the monodispersed Gaussian chain:

$$P_i(u) = \frac{2}{u^2}[\exp(-u) - 1 + u] \tag{5}$$

where $u = q^2(R_g)_i^2$, and $(R_g)_i^2$ is the mean square radius of gyration. In practice, since LDPE used in this work has wide molecular weight distribution, Eq. (5) should be modified to take the polydispersity into account. Assuming that it has Schultz-Zimm-type molecular weight distribution, finally the structure factor for a mixture of polydispersed polymers is given as follows [29,30]:

$$\frac{1}{S(q)} = \frac{1}{\nu_D\phi_D N_D^n g_D(u)} + \frac{1}{\nu_H\phi_H N_H^n g_H(u)} - \frac{2\chi}{\nu} \tag{6}$$

where N_i^n is the number-average degree of polymerization and $\nu = (\phi_H/\nu_H + \phi_D/\nu_D)^{-1}$. $g_i(x)$ is given by

$$g_i(x) = \frac{2}{x^2}\left[x - 1 + \left(\frac{h_i}{h_i + x}\right)^{h_i}\right] \tag{7}$$

where $x = q^2(R_g^n)_i^2$ and $(R_g^n)_i^2$ is the number-average radius of gyration and h_i is defined by

$$h_i = \left(\frac{N_i^w}{N_i^n} - 1\right)^{-1} \tag{8}$$

where N_i^w andN_i^n is the weight- and number-average degree of polymerization, respectively.

Slow cooling may cause phase segregation due to major differences in the crystallization kinetics. When there is a phase segregation in a blend, the following equation has been used [31,32], and its feasibility experimentally proved by Wignall et al. [19]:

$$\frac{d\Sigma}{d\Omega}(q) = \frac{8\pi a_1^3\phi_1\phi_2(\rho_1 - \rho_2)}{(1 + q^2a_1^2)^2} \tag{9}$$

where a_1 is the correlation length characterizing the spatial dimensions via an exponential correlation function and φ_i is the volume fraction of ith component. Eq. (5) is called the Debye–Bueche equation.

3. Results and discussion

Fig. 1 shows the SANS and SAXS profiles for a slowly cooled O-*m*LLDPE(D)/LDPE(H) = 10/90 sample; the two scattering profiles are quite different. The nanoscale density fluctuation in the sample is the origin of the scattering signals for both SAXS and SANS. However, in SANS there is an additional scattering due to the non-homogeneous distribution of the deuterated component on the nanoscale. The hydrogenated sample has a well-developed lamellar structure, but exhibits almost no coherent scattering in SANS because of the low scattering length density of the hydrogen atom, which suggests that the coherent neutron scattering caused by the density fluctuation of the hydrogenated sample should be almost

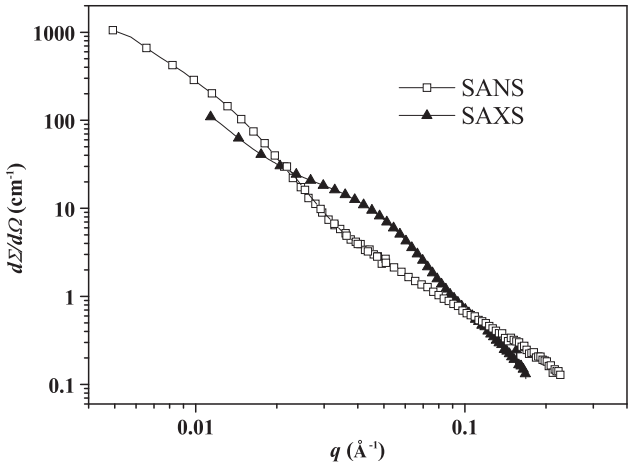

Fig. 1. SANS and SAXS scattering profiles for an O-*m*LLDPE(D)/LDPE(H) = 10/90 blend sample cooled slowly from 145 °C at 0.5 °C/min.

negligible compared to that of the incoherent background. The SANS coherent cross section of a 100% deuterated sample is proportional to that of SAXS with a theoretical ratio of 1/1.27 [33]. In the case of D/H blends, the SANS data is expected to exhibit Debye–Bueche (DB) behavior if there is a phase separation of the deuterated and hydrogenated components or RPA behavior if the mixture is homogeneous regardless of the crystallinity of the blends. When either the deuterated or hydrogenated component is preferentially located in the crystalline lamellae, the SANS curve for the sample is expected to be similar to the SAXS curve (see Fig. 5 for the D/H = 90/10 sample), i.e., to consist of a broad small angle scattering peak due to lamellar stacking, which is known as the Bragg scattering. The intensity of the Bragg scattering in the SANS profile depends on the distribution of the deuterated component, which is calculated later in this paper. In Fig. 1, only Bragg scattering is present in the SAXS profile, whereas DB-type scattering is dominant in the SANS profile and there is no Bragg scattering.

Fig. 2 shows the SANS profiles of the slowly cooled and quenched O-*m*LLDPE(D)/LDPE(H) = 30/70 sample. As we have shown previously, the scattering of the quenched sample is RPA-type, which is characteristic of a homogeneous mixture of a D/H polymer [18]. There are two kinds of asymptotic behavior in the slowly cooled sample; the exponents of the power-law, $d\Sigma/d\Omega \sim q^{-n}$, derived from the low-$q$ upturn (the low-q side of $q \sim 0.027$ Å^{-1}) and the high-q region are n ~ 3.68 and 1.89, respectively. Low-q regions are well described by the Debye–Bueche formalism Eq. (9) and its fitting in Fig. 3: the Porod exponent 3.68 indicates the presence of sharp interphase boundaries [34] between the two phases; one phase contains more deuterated component than the other phase. The slight deviation of the Porod exponent from the ideal value 4 may be due to minor surface roughness of the interface boundary, but the difference is insignificant. Note that the quenched sample does not produce this DB-type scattering, which suggests that there is no macrophase separation. The exponent 1.89 for the high-q region is characteristic of RPA scattering from a homogeneous mixture, which indicates that the slowly cooled sample also contains a homogeneous mixing region, although the composition of D/H in this region might not be 30/70. This result demonstrates that there are both segregated and homogeneous regions in the slowly cooled D/H = 30/70 sample.

SANS profiles obtained from slowly cooled samples of various compositions (open symbols) are shown in Fig. 4 with arbitrary scales for clarity and are compared with those of the quenched ones (closed symbols). Apart from the results for the O-*m*LLDPE(D)/LDPE

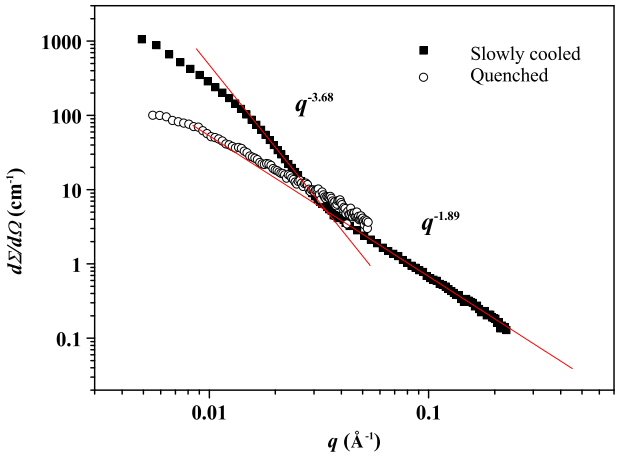

Fig. 2. SANS scattering profile for an O-*m*LLDPE(D)/LDPE(H) = 30/70 blend sample cooled slowly at 0.5 °C/min (closed squares) and quenched (open circles) from 145 °C.

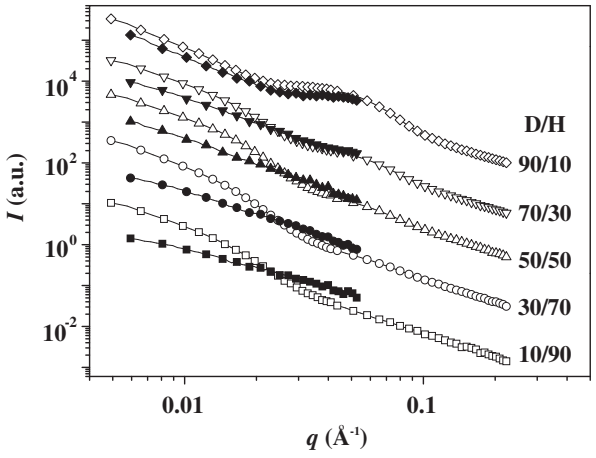

Fig. 4. SANS profiles for a series of slowly cooled (open) and quenched (closed) O-*m*LLDPE(D)/LDPE(H) blend samples.

(H) = 90/10 blend, the scattering profiles of slowly cooled samples contain two distinct regions corresponding to DB-type scattering in the low q-region and Bragg- or RPA-type scattering in the high q-region. The intensities of the Bragg peaks obtained from the long period increase with increases in the fraction of O-*m*LLDPE(D) in the blend. On the other hand, DB-type scattering is less distinguishable from RPA-type scattering as the content of D increases. The DB fitting results are summarized in Table 2 along with the long periods calculated from the SAXS and SANS profiles; it is noted that SAXS profiles of all compositions are not much different from that in Fig. 1 except for peak positions and intensities (all of the SAXS data are not shown). The deviations of the zero angle scattering intensities from the ideal values, which were calculated by making the assumption of perfect segregation, suggest that this assumption is not valid; note also the presence of the homogeneous mixing regions indicated by RPA scattering. The correlation lengths obtained from the SANS profiles are on the order of the long period and are not composition-dependent. These results from DB analysis suggest that there may be phase separations between D and H polymers but their domain size may be more likely nanoscale rather than macroscale. In order to understand this nanoscale phase-separated structure, we further analyzed the Bragg scattering in detail. Although the long periods obtained from the SAXS profiles are not composition-dependent, those from the SANS profiles, which are mainly due to the deuterated components, do increase with increases in the fraction of O-*m*LLDPE(D). The scattering intensity multiplied by q^2, or the Lorentz-corrected intensity, is plotted in Fig. 5. The O-*m*LLDPE(D)/LDPE(H) = 90/10 sample produces a slight bump at the q position where the SAXS peak is located, but its peak maximum position appears at higher q position than that of SAXS peak. The SANS peak position of the D/H = 70/30 sample is shifted further to higher q with respect to the SAXS peak position of the 90/10 sample. It is noted that the long periods in the SAXS profiles of 90/10 and 70/30 are almost the same as shown in Table 2. This result is good evidence of phase segregation because perfectly homogeneous mixtures will produce the same peak positions in SAXS with those in SANS regardless of the composition; the peak in SANS is mainly originated from the lamellar stack containing D components whereas that in SAXS is from any lamellar stack. This suggests the followings. O-*m*LLDPE(D) crystallized in the phase-separated domains has a smaller long period and thus a smaller lamellar thickness than that in pure O-*m*LLDPE. The lamellar stacks containing significant amount of D-component is phase-separated from those of the pure H polymer (note that pure H polymer shows higher crystallinity than the pure D polymer but the lamellar stack of pure H polymer is not visible in SANS at all).

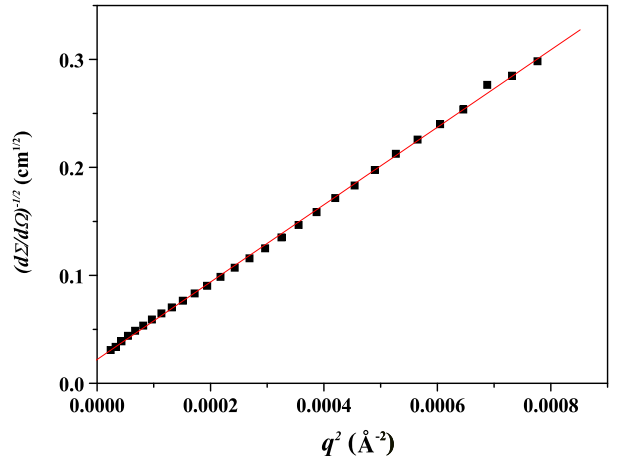

Fig. 3. Debye–Bueche plots of low-q region for an slowly cooled O-*m*LLDPE(D)/LDPE(H) = 30/70 blend sample.

The invariants of the SANS profiles were analyzed for the low-q DB scattering region and the Bragg scattering regions separately. We first discuss the low-q DB-type scattering region. To integrate the intensity of the DB-type scattering, we subtracted the RPA scattering and assumed that the Bragg intensity is of lesser

Table 2
Parameters of O-*m*LLDPE(D)/LDPE(H) blends evaluated at room temperature.

$f_{w,D}$[a]	Vol. fractions		Correl. Length, a_1 (Å)	$10^3 d\Sigma/d\Omega$ ($q = 0$) (cm^{-1})		Long period (Å)[d]	
	φ_D	φ_H		Exp.[b]	Calc.[c]	SANS	SAXS
0.1	8.3	91.7	128.0	9.5	28.1	–	142.2
0.3	26.0	74.0	149.7	55.8	113.1	–	140.2
0.5	45.0	55.0	125.7	38.0	86.2	102	145.2
0.7	65.6	34.4	130.1	33.0	87.1	108	145.2
0.9	88.0	12.0	–	–	–	119	145.2

[a] The weight fraction of O-*m*LLDPE(D) in blends.
[b] Calculated from Debye–Bueche plot and linear fitting.
[c] Calculated for the perfect segregation with the fitted a_1 values and volume fractions.
[d] Calculated from the maximum peak position of the Lorentz-corrected profiles.

Table 3
Invariants and the calculated contrast for O-*m*LLDPE(D)/LDPE(H) blends.

$f_{w,D}$[a]	Q_{exp} (cm^{-1} $Å^{-3}$)[b]	ρ_0 ($\times 10^{-13}$ $-cm^2$)	$(\rho_1-\rho_0)^2$ ($\times 10^{-26}$ cm^{-4})	$(\rho_2-\rho_0)^2$ ($\times 10^{-26}$ cm^{-4})	$(\rho_1-\rho_2)^2$ ($\times 10^{-26}$ cm^{-4})
0.1	5.4E-4	0.078	1.431	0.018	
0.3	1.9E-3	0.343	0.866	0.159	
0.5	2.5E-3	0.609	0.442	0.442	1.767
0.7	1.5E-3	0.875	0.159	0.866	
0.9	< 2.8E-4	1.141	0.018	1.431	

[a] The weight fraction of O-*m*LLDPE(D) in blends.
[b] Calculated invariants after subtracting the calculated RPA scattering which assume the same parameters with the quenched sample but is scaled to match the highest angle intensities of the slowly cooled sample.

importance in the DB-type scattering region, $q < 0.027$ $Å^{-1}$. The data were then extrapolated to '$q = 0$' and 'q → infinite' with the Guinier and Porod approximations respectively. The invariant values (Q) experimentally obtained for the low-q side are listed in Table 3.

The invariant is related to the structural parameters as follows [27]:

$$\begin{aligned} Q_{ij} &= 2\pi^2\varphi_i\varphi_j k_{ij} \\ k_{ij} &= \left(\rho_i - \rho_j\right)^2 \\ Q &= \sum_{i=0,i\neq j}^{N-1} Q_{ij} \end{aligned} \tag{10}$$

where φ_i and φ_j are the volume fraction of ith and jth component, respectively. $k_{ij}$is the contrast between i and j component of which scattering length density is ρ_i and ρ_j, respectively.

The scattering length densities of the crystalline and amorphous regions of the homopolymer are not significantly different, so we assumed there are only three domains: the homogeneous mixture, pure O-*m*LLDPE(D), and pure LDPE(H), with indexes of 0, 1, and 2, respectively. The calculated contrasts are shown in Table 3. When the weight fraction ($f_{w,D}$) is 0.1, the contrast between the pure LDPE (H) domain and the homogeneous mixture is negligible compared to that between the other domains, suggesting that there must be a phase-segregated pure O-*m*LLDPE(D) domain that is responsible for the DB-type scattering of the sample. With these assumptions, the volume fraction of O-*m*LLDPE(D) was calculated from the invariant by using Eq. (10) and found to be approximately 1%. When $f_{w,D}$ is 0.9, the segregation of pure LDPE(H) is mainly responsible for the scattering and its volume fraction is calculated to be less than 0.5%. When $f_{w,D} = 0.5$, the calculated volume fraction of either the O-*m*LLDPE(D) domain or the LDPE(H) domain reaches approximately 10%. By reviewing the results for the various compositions, we conclude that this kind of macrosopic phase segregation is not significant, and that the volume fractions of the phase-segregated domains are lower than those of the crystalline domains, which implies the presence of extensive cocrystallization.

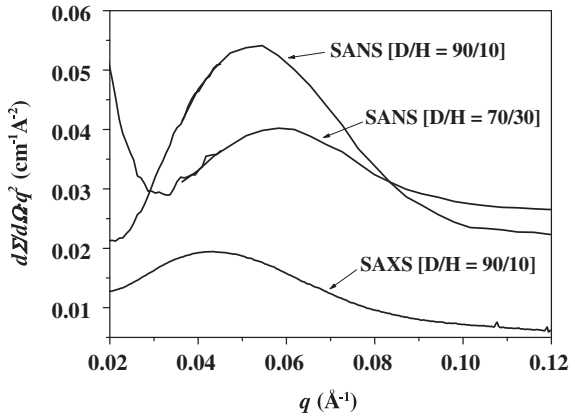

Fig. 5. Lorentz-corrected SANS and SAXS profiles for D/*H* = 90/10 and 70/30 blends.

The segregation behavior within the crystalline lamellar structure can be determined from the invariant calculated for the Bragg scattering region, $q > 0.027$ $Å^{-1}$. We subtracted the RPA scattering in the region and assumed that the DB scattering is of lesser importance in the region because it decreases proportionally to q^{-4}. In this section, instead of calculating the structural parameters from the invariant of the Bragg scattering, we compared the experimental values to the calculated values for two different scenarios: perfect macrophase separation and perfect cocrystallization. The invariants for the two cases can be calculated by using Eq. (10) under the assumption of the two-phase structure of the lamellar stack model, where φ_1 and φ_2 are the volume fractions of the lamellae and the interlamellar amorphous region respectively.

If the relative composition of deuterated molecule in each region is same, which means the perfect homogeneity, the invariant calculated from SAXS and SANS will be proportional to each other with the following relation:

$$Q_{SANS} = (Q_{SAXS}\cdot k_{SANS})/k_{SAXS} \tag{11}$$

where k is the contrast of the crystalline structure to the each light source.

In contrast, when there is perfect segregation that results in macrophase separated domains, each domain will contain its own crystalline structure. The Bragg intensity will then be proportional to the volume fraction of the deuterated component, and O-*m*LLDPE(D) will have its usual characteristic crystallinity in its domain.

For such a case, SANS invariant can be calculated as following:

$$Q_{SANS} = \left(Q_{SAXS}x_{c,d}(1-x_{c,d})\right)/(x_c(1-x_c))\cdot\left(f_{v,D}/C\right) \tag{12}$$

where C is the ratio of the SANS and SAXS scattering cross sections for a pure deuterated polymer, which is 1.27 in this work. $f_{v,D}$ is the volume fraction of deuterated component. x_c and $x_{c,d}$ are crystallinity of blend sample and O-*m*LLDPE(D), respectively.

The experimental and calculated invariant values are shown in Fig. 6. For low fractions of O-*m*LLDPE(D), the experimental SANS invariants are close to that of the perfect cocrystal structure (see the closed circles in Fig. 6). As the deuterated fraction increases, the SANS invariant deviates from that of perfect cocrystallization, but remains between the values of the two extreme scenarios. For $f_{w,D} = 0.9$, the SANS invariant is even larger than that of the perfect segregated structure, which suggests that LDPE(H) is preferentially located between O-*m*LLDPE(D)-rich lamellae rather than in macrophase segregation. This result indicates that O-*m*LLDPE(D) and LDPE(H) blends tend to cocrystallize in compositions with less deuteration. Although phase separation is observed with increases in the O-*m*LLDPE fraction, it occurs on the lamellar scale or long

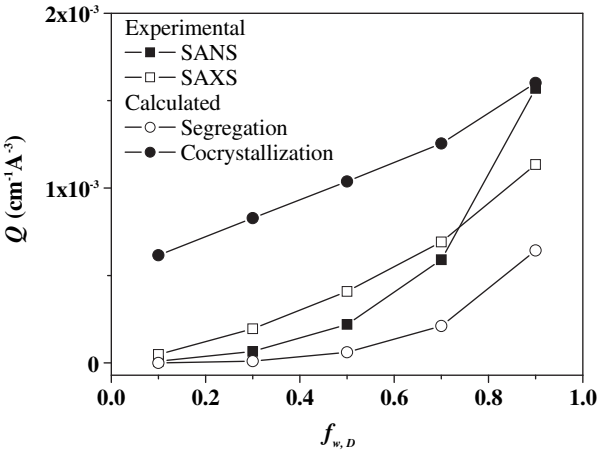

Fig. 6. SANS (a) and SAXS (b) invariants calculated from the Bragg peak at q~0.027 Å^{-1} and SANS invariants calculated from the SAXS invariants by assuming perfect segregation (c) and perfect cocrystallization (d) (see text).

period scale, such that the O-*m*LLDPE rich lamellae and LDPE(H) rich interlamellar amorphous region. The shift of the long period in the SANS data (see Table 3) observed for $f_{v,D} \geq 0.5$ suggests the formation of thicker O-*m*LLDPE(D)-rich lamellae with increases in the fraction of O-*m*LLDPE(D). However, the position of that peak in the SAXS profiles does not vary with the composition. This result suggests that the peak in the SAXS profiles is associated with cocrystallized lamellae or LDPE(H)-rich lamellae, and that the peak in the SANS profiles is due to O-*m*LLDPE(D)-rich lamellae that are surrounded by LDPE(H)-rich amorphous regions. A peak due to a pure O-*m*LLDPE(D) macrophase segregated domain would be located at the same q in both SANS and SAXS. Considering the results from the analysis of the DB-type scattering that demonstrates phase separation in samples with compositions of less deuteration, we conclude that LDPE(H) forms macrophase separated lamella stacks in such samples, whereas the O-*m*LLDPE(D) component forms extensive cocrystals with the remaining LDPE(H) that does not macroseparate. With increases in the deuterated fraction, nanoscale separation arises through the formation of O-*m*LLDPE-rich lamellae rather than through macrophase separation.

The DSC endotherms for the slowly cooled blends shown in Fig. 7 were obtained at a heating rate of 10 °C/min. The melting temperature of O-*m*LLDPE(D) is lower by approximately 9 °C than that of LDPE(H) due to its deuteration [17] and the number of short-chain branches in octene-LLDPE [35]. The melting endotherm of pure O-*m*LLDPE(D) is found for all compositions at the same temperature, around 100 °C, and its intensity does not significantly vary with composition, as summarized in Table 4 with the crystallinities. However, the LDPE(H) endotherms shift to lower temperatures as the fraction of O-*m*LLDPE(D) increases. When $f_{w,D}$ is larger than 0.7, no peak is found at the endotherm position of pure LDPE(H). This result is consistent with the scattering results, which suggests the presence of extensive cocrystallization in blends with lower fractions of O-*m*LLDPE(D). The separation of two components from DSC thermograms is described with the data of D/H = 30/70 sample as an example in the following paragraph.

To estimate the crystallinity of O-*m*LLDPE(D) in the blend with D/H = 30/70, the melting endotherm of the D/H = 30/70 sample was linearly interpolated (Fig. 8a) between those of pure O-*m*LLDPE (D) (Fig. 8b) and pure LDPE(H) (Fig. 8c); the melting endotherm of pure O-*m*LLDPE(D) was calculated by scaling that of the D/H = 90/10 sample with the weight fraction of the deuterated component. The heat of fusion of O-*m*LLDPE(D) component in the 30/70 blend is

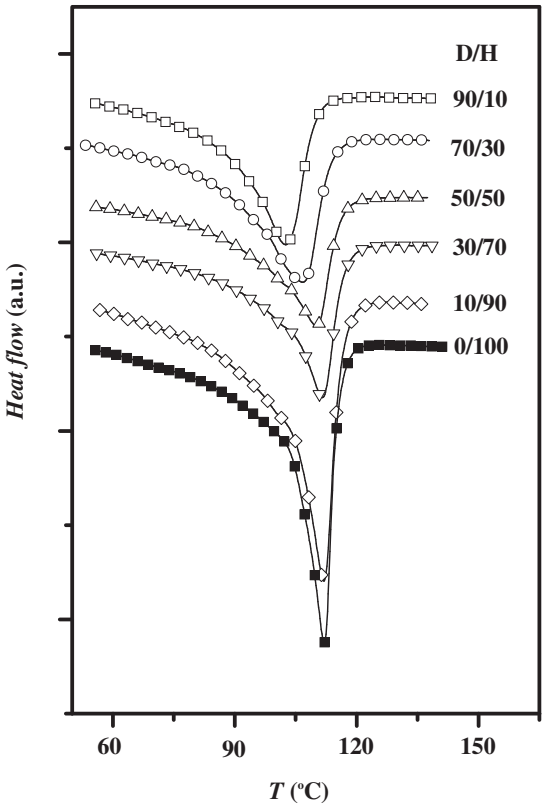

Fig. 7. DSC thermograms of a series of slowly cooled O-*m*LLDPE(D)/LDPE(H) blend samples. A heating rate of 10 °C/min was used in these measurements.

about 12% of that of the D/H = 30/70 sample. The interpolated curve satisfactorily matches the D/H = 30/70 thermogram, which suggests that O-*m*LLDPE(D)-rich lamellae are present as well as LDPE(H)-rich regions. Careful examination, however, of the 30/70 thermogram reveals the strong peak evolved between the two peaks due to O-*m*LLDPE and LDPE, which supports the presence of cocrystal.

The mass fraction of crystalline O-*m*LLDPE(D) that is responsible for the peak near 100 °C in the DSC thermogram can be estimated by taking into account the density of the O-*m*LLDPE(D) lamellae and the amorphous region, which are approximately 4% and 8% for the D/H = 10/90 and 30/70 samples respectively under the assumption that CD_2 and CH_2 crystals have the same heat of fusion. These values are larger than the volume fractions of the phase-separated O-*m*LLDPE(D) that were calculated from the SANS invariants as discussed above, which were approximately 1% and 3% respectively. This result suggests that most of the O-*m*LLDPE(D)-rich lamellae are located outside the O-*m*LLDPE(D)-rich phase-segregated domains, or in other words the O-*m*LLDPE(D)-rich lamellae are surrounded by

Table 4
Crystallinity and melting temperature of O-*m*LLDPE(D)/LDPE(H) blends calculated from DSC thermograms.

$f_{w,D}$[a]	Crystallinity (wt.%)	T_m (°C)	
		A	B
0.1	35.9	102.2	112.1
0.3	31.8	102.8	111.6
0.5	27.7	102.3	110.2
0.7	28.7	102.9	107.0
0.9	26.7	102.3	104.6

[a] The weight fraction of O-*m*LLDPE in blends.

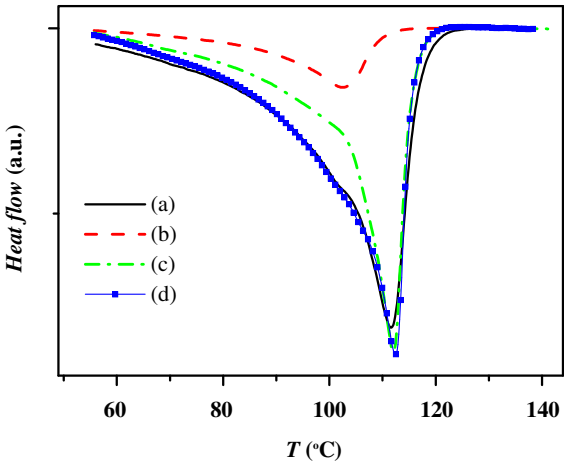

Fig. 8. Separation of the O-*m*LLDPE(D) fraction from the DSC thermogram for a slowly cooled D/H = 30/70 blend: (a) DSC thermogram of the 30/70 blend; (b) approximate thermogram of the O-*m*LLDPE(D) fraction calculated from that of the 90/10 blend; (c) scaled thermogram of LDPE(H); (d) sum of (b) and (c).

relatively homogeneously mixed or LDPE(H)-rich amorphous regions, which is consistent with the SANS analysis of the Bragg scattering discussed above.

In summary, O-*m*LLDPE(D) is segregated on the nanoscale in separated lamellae in the LDPE(H)-rich compositions instead of in macrophase-segregated domains. As the fraction of O-*m*LLDPE(D) increases, both the cocrystallized lamellar stacks and stacks with O-*m*LLDPE(D) lamellae and LDPE(H)-rich interlamellar amorphous regions are formed. Such composition-dependent cocrystallization behavior is also found for the HDPE/LLDPE blend system [17,19]. This result can be explained as follows. In a blend of two polymers with different crystallization temperatures, when the content of the component with the higher crystallization temperature (LDPE (H) in this study) is high, it tends to crystallize first, and on subsequent cooling the remaining LDPE(H) and O-*m*LLDPE(D) either cocrystallize or remain in a homogeneous amorphous mixture. As the content of LDPE(H) decreases, the LDPE(H) chains become less likely to form their own lamellae because LDPE(H) is surrounded by the other component in the melt state, as we demonstrated in a previous study. Thus kinetics has a significant role in the cocrystallization of blends and we have also shown that fast cooling can prevent phase separation of this blend.

4. Conclusions

In this study the morphological structures of blends of O-*m*LLDPE(D) and LDPE(H) were found to be composition-dependent by using a method that combines SANS and SAXS. These blends exhibit composition-dependent cocrystallization and phase segregation behaviors, with the following resulting morphologies. O-*m*LLDPE(D) is segregated in separated lamellae in blends with LDPE (H)-rich compositions. As the fraction of O-*m*LLDPE(D) increases, it forms both cocrystals in which the LDPE(H) fraction is less than the average and separated lamellae. Although phase segregation does occur during crystallization, its fraction is quite small: approximately 60% of the amorphous regions in the blends are homogeneous.

Acknowledgments

This study was supported by the Ministry of Education, Science & Technology (MEST) (Basic Research Grant of Nuclear Energy, Grant 20090060053, KISTEP, World Class University Program, and BK21 Program) and by the National Research Foundation (NRF) of Korea (Center for Electro-Photo Behaviors in Advanced Molecular Systems). The synchrotron X-ray scattering measurements at Pohang Light Source were supported by MEST, POSCO, and POSTECH Foundation. This work was also benefited from the Argonne National Laboratory funded by the U.S. DOE-BES under Contract No. DE-AC02-06CH11357.

References

[1] Nwabunma D, Kyu T. Polyolefin blends. New York: Wiley; 2007.
[2] Peacock AJ. Handbook of polyethylene: structures, properties and applications. New York: Marcel Dekker, Inc.; 2000.
[3] Wardhaugh LT, Williams MC. Polym Eng Sci 1995;35:18–27.
[4] Hill MJ, Puig CC. J Appl Polym Sci 1997;65:1921–31.
[5] Gabriel C, Kaschta J, Munstedt H. Rheol Acta 1998;37:7–20.
[6] Munstedt H, Kurzbeck S, Egersdorfer L. Rheol Acta 1998;37:21–9.
[7] Wignall GD, Alamo RG, Ritchson EJ, Mandelkern L, Schwahn D. Macromolecules 2001;34:8160–5.
[8] Usami T, Gotoh Y, Takayama S. Macromolecules 1986;19:2722–6.
[9] Liu C, Wang J, He J. Polymer 2002;43:3811–8.
[10] Yilmazer UJ. Appl Polym Sci 1991;42:2379–84.
[11] Hakin J. (Petrolite Corporation.) US Pat. 1998;4:764,326.
[12] Lu J, Sue H-J. J Polym Sci Part B Polym Phys 2002;40:507–18.
[13] Hameed T, Hussein IA. Polymer 2002;43:6911–29.
[14] Hussein IA, Williams MC. Polym Eng Sci 2004;44:660–72.
[15] Niaounakis M, Kontou E. J Polym Sci Part B Polym Phys 2005;43:1712–27.
[16] Fang Y, Carreau PJ, Lafleur PG. Polym Eng Sci 2005;45:1254–64.
[17] (a) Tashiro K, Stein RS, Shaw LH. Macromolecules 1992;25:1801–8;
(b) Tashiro K, Izuchi M, Kobayashi M, Stein RS. Macromolecules 1994;27:1221–7;
(c) Tashiro K, Izuchi M, Kobayashi M, Stein RS. Macromolecules 1994;27:1228–33;
(d) Tashiro K, Izuchi M, Kaneuchi F, Jin C, Kobayashi M, Stein RS. Macromolecules 1994;27:1240–4.
[18] Shin TJ, Lee B, Lee J, Jin S, Sung BS, Han YS, et al. J Appl Crystallogr 2009;42:161–8.
[19] Wignall GD, Londono JD, Lin JS, Alamo RG, Galante MJ, Mandelkern L. Macromolecules 1995;28:3156–67.
[20] Tashiro K, Imanishi K, Izuchi M, Kobayashi M, Itoh Y, Imai M, et al. Macromolecules 1995;28:8484–90.
[21] (a) Bolze J, Kim J, Huang J-Y, Rah S, Youn HS, Lee B, et al. Macromol Res 2002;10:2–12;
(b) Heo K, Yoon J, Jin KS, Jin S, Kim G, Sato H, et al. J Appl Crystallogr 2007;40:s594–8;
(c) Heo K, Yoon J, Jin KS, Jin S, Sato H, Ozaki Y, et al. J Phys Chem B 2008;112:4571–81;
(d) Jin KS, Park JK, Yoon J, Rho Y, Kim J-H, Kim EE, et al. J Phys Chem B 2008;112:9603–12;
(e) Jin S, Higashihara T, Watanabe T, Jin KS, Yoon J, Heo K, et al. Macromol Res 2008;16:686–94;
(f) Jin KS, Rho Y, Kim J, Kim H, Kim IJ, Ree M. J Phys Chem B 2008;112:15821–7;
(g) Jin KS, Shin SR, Ahn B, Heo K, Kim SJ, Ree M. J Phys Chem B 2009;113:1852–6;
(h) Shin SR, Jin KS, Lee CK, Spinks GM, Baughman RH, So I, et al. J Adv Mater 2009;21:1907–10;
(i) Jin KS, Shin SR, Ahn B, Jin S, Rho Y, Kim H, et al. J Phys Chem B 2010;114:4783–8.
[22] (a) Yoon J, Kim KW, Kim J, Heo K, Jin KS, Jin S, et al. Macromol Res 2008;16:575–85;
(b) Lee B, Park Y-H, Hwang YT, Oh W, Yoon J, Ree M. Nat Mater 2005;4:147–50;
(c) Lee B, Oh W, Hwang Y, Park Y-H, Yoon J, Jin KS, et al. Adv Mater 2005;17:696–701;
(d) Lee B, Yoon J, Oh W, Hwang Y, Heo K, Jin KS, et al. Macromolecules 2005;39:3395–405;
(e) Lee B, Oh W, Yoon J, Hwang Y, Kim J, Landes BG, et al. Macromolecules 2005;38:8991–5;
(f) Lee B, Park I, Yoon J, Park S, Kim J, Kim K-W, et al. Macromolecules 2005;38:4311–23;
(g) Heo K, Park S-G, Yoon J, Jin KS, Jin S, Rhee S-W, et al. J Phys Chem C 2007;111:10848–54;
(h) Yoon J, Lee SW, Choi S, Heo K, Jin KS, Jin S, et al. J Phys Chem B 2008;112:5338–49.
[23] (a) Ree M, Ko IS. Phys High Tech 2007;14:2–7;
(b) Ree M, Nam SH, Yoon M, Kim B, Kim K-R, Kang T-H, et al. Synchrotron Radiat News 2009;22:4–12.
[24] Quinn Jr FA, Mandelkern L. J Am Chem Soc 1958;80:3178–82.

[25] Schipp C, Hill MJ, Barham PJ, Cloke VM, Higgins JS, Oiarzabal L. Polymer 1996;37:2291–7.
[26] Agamalian M, Alamo RG, Kim MH, Londono JD, Mandelkern L, Wignall GD. Macromolecules 1999;32:3093–6.
[27] Wignall GD, Alamo RG, Londono JD, Mandelkern L, Kim MH, Lin JS, et al. Macromolecules 2000;33:551–61.
[28] Brandrup J, Immergut EH. Polymer handbook. New York: John Wiley; 1975.
[29] Glatter O, Kratky O. Small-angle X-ray scattering. New York: Academic; 1982.
[30] Balsara NP, Lohse DJ, Graessley WW, Krishnamoorti RJ. J Chem Phys 1994;100:3905–10.
[31] Debye P, Bueche AM. J Appl Phys 1949;20:518–35.
[32] Debye P, Anderson HR, Brumberger H. J Appl Phys 1957;28:679–83.
[33] Russell TP, Lin JS, Wignall GD. J Appl Cryst 1988;21:629–38.
[34] Alamo RG, Graessley WW, Krishnamoorti R, Lohse DJ, Londono JD, Mandelkern L, et al. Macromolecules 1997;30:561–6.
[35] Yamaguchi M, Abe S. J Polym Sci Part B Polym Phys Ed 1999;74:3153–9.